Suplemento de la Revista Mexicana de Física **4** 021117 (2023) 1–5

DM-SM interactions mediated by spin-one particles: EFT study

F. Fortuna

Centro de Investigación y de Estudios Avanzados del Instituto Politécnico Nacional
Apartado Postal 14-740, 07000, Ciudad de México, México.

Received 25 May 2023; accepted 27 July 2023

Standard model-dark matter particles, mediated by spin one fields, are analyzed within the effective field theory framework. We [1, 2] consider dark particles masses from few MeV to 6.4 TeV. We restrict the EFT using bounds from relic density, Z invisible decay width, direct and indirect detection limits and collider constraints. Solutions below m_Z are found for two operators. Others, around the electroweak scale or slightly above, are also compatible with all present limits.

Keywords: Dark matter; effective field theory.

DOI: https://doi.org/10.31349/SuplRevMexFis.4.021117

1. Introduction

The dark sector comprises $\sim 95\%$ of the universe, but only its gravitational effects have been measured. The nature of dark energy and Dark Matter (DM) remains as one of the most puzzling challenges of today's Physics. Although the dynamics underlying dark energy may be at too-large energy scales for high-energy physics measurements, it might be that DM could be probed in our current and forthcoming particle physics experiments, provided it also has non-gravitational interactions. Although motivated DM candidates masses span ~ 40 orders of magnitude, weakly interacting massive particles (WIMP) [3, 4] have been historically preferred, as they can avoid direct detection limits and generate a relic abundance matching the one derived from cosmic microwave background radiation measurements (which requires perturbative annihilation cross sections in the range of the electroweak interactions). We follow this WIMP paradigm within the most general description provided by the effective field theory (EFT) approach [5-11]: the SM degrees of freedom and symmetries are used in the EFT, assuming that the mediator mass is heavy compared to the DM and SM particles. Specifically, our EFT, for DM-SM interactions mediated by heavy particles, was derived in Ref. [12]. We restrict our analysis to spin-one mediators, that have been less studied in the literature.

In Sec. 2 our EFT [12] is introduced, highlighting the relevant part of this study. Bounds from the invisible Z decay width and from the observed relic abundance are derived in Sec. 3. In Sec. 4 observational limits are worked out: in Subsec. 4.1 (4.2) (in)direct detection bounds are given. Collider constraints are treated in Sec. 5. Section 6 concludes this contribution.

2. Effective Field Theory

The dark sector must contain a stable particle, acting as DM. So we will assume [13, 14] that there is a (unspecified) symmetry group, $\mathcal{G}_{\rm DM}$ group under which all the dark fields transform in a non-trivial manner, whilst all SM particles will be $\mathcal{G}_{\rm DM}$ singlets. Then, under the SM local gauge symmetry group, $\mathcal{G}_{\rm SM} = SU(3) \otimes SU(2) \otimes U(1)$, the dark fields would be singlets. DM-SM interactions mediated by the exchange of heavy particles (singlets under $\mathcal{G}_{\rm DM} \times \mathcal{G}_{\rm SM}$) are studied within this EFT.

Dark sector may comprise vectors, X, fermions, Ψ, and scalars, Φ. Within the WIMP paradigm, spin-one mediators need to be feebly coupled to DM and SM particles, as encoded in the effective coefficients $C_{\rm eff}$. Our EFT includes operators of mass dimension ≤ 6. Models with fermion and scalar mediators have already been extensively studied in the literature [9,10,15-24], therefore we focus on spin-1 mediators (antisymmetric tensors and vectors).

It is convenient to split our interaction Lagrangian as:

- Dark fermions (Ψ) terms:

$$\mathcal{L}^{\Psi}_{\rm eff} = \frac{\Upsilon_{\rm eff}}{\Lambda} B_{\mu\nu} \bar{\Psi} \sigma^{\mu\nu} \Psi + \frac{A^{L,R}_{\rm eff}}{\Lambda^2} \bar{\psi} \gamma_\mu \psi \bar{\Psi} \gamma^\mu P_{L,R} \Psi + \frac{\kappa^{L,R}_{\rm eff}}{\Lambda^2} B_{\mu\nu} \bar{\Psi} \left(\gamma^\mu \overleftrightarrow{\mathcal{D}}^\nu - \gamma^\nu \overleftrightarrow{\mathcal{D}}^\mu \right) P_{L,R} \Psi. \quad (1)$$

- Dark bosons (Φ, X) terms:

$$\mathcal{L}^{\Phi,X}_{\rm eff} = \frac{\zeta_{\rm eff}}{\Lambda} B_{\mu\nu} X^{\mu\nu} \Phi + \frac{\epsilon_{\rm eff}}{\Lambda^2} \bar{\psi} \gamma_\mu \psi \frac{1}{2i} \Phi^\dagger \overleftrightarrow{\mathcal{D}}^\mu \Phi \,, \quad (2)$$

where $B_{\mu\nu}$ stands for the $U(1)_Y$ field-strength tensor, ψ for SM fermions and universal couplings to the SM fermions are assumed.

In the following we typically use the single operator dominance hypothesis. We also consider combined effects of the appropriate operators.

3. Relic density and invisible decay width

Using our EFT, we employ micrOMEGAs code [25] to calculate the dark matter relic density. Coefficients in the effective

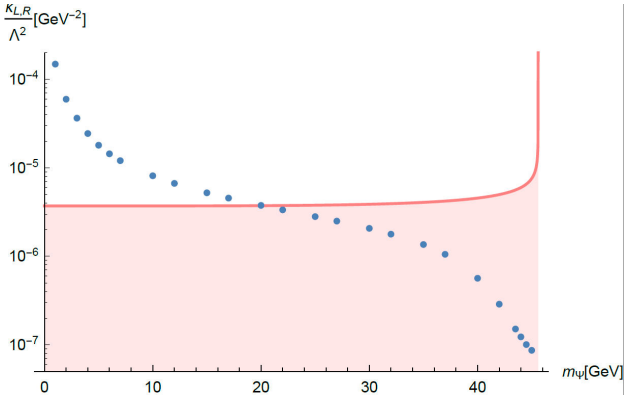

FIGURE 1. $\kappa^{L,R}_{\rm eff}/\Lambda^2$ compatible with the observed relic density (blue dots) and the invisible Z decay width (pink area), depending on the dark fermion mass.

Lagrangians, in Eqs. (1) and (2), are determined so that the observed relic abundance [26] is correctly reproduced

$$\Omega_{\rm DM}h^2 = 0.1200 \pm 0.0012\,. \tag{3}$$

For $m_{\rm DM} < m_Z/2$, the invisible Z decay width sets relevant restrictions on the parameters of our Lagrangian in Eqs. (1) and (2). Reference [27] improved Bhabha scattering $e^+e^- \to e^+e^-$ computation, modifying correspondingly the number of light active neutrinos; which is now $N_\nu = (2.9975 \pm 0.00074)$.

Accordingly, the experimental value of the invisible decay width of the Z boson results in $\Gamma_Z^{\rm inv} = (501.03 \pm 1.27)$ MeV, which includes the SM decays to neutrino pairs as well as any other possible unobserved contributions.

In the SM, the partial decay rate to a neutrino pair is $\Gamma(Z \to \bar\nu\nu) = (167.15 \pm 0.01)$ MeV [28]. With three light neutrinos with standard couplings to the Z, this yields $\Gamma_Z^{\rm inv} - \Gamma_Z^{\bar\nu\nu} = (-0.42 \pm 1.30)$ MeV. Thus, we employ

$$\Gamma_Z^{\rm inv} - \Gamma_Z^{\bar\nu\nu} = 2.13 \text{ MeV} \;\; \text{at} \;\; 95\%\text{CL}\,. \tag{4}$$

The $B_{\mu\nu}\bar\Psi\sigma^{\mu\nu}\Psi$ operator in Eq. (1) yields $Z \to \bar\Psi\Psi$, allowing us to bind $\Upsilon_{\rm eff}/\Lambda = (\Upsilon_{\rm eff}/\Lambda)(\Gamma_{Z\to\bar\Psi\Psi}, m_\Psi)$.

Using Eq. (4) for $\Gamma_{Z\to\bar\Psi\Psi}$, we computed the region allowed in the $m_\Psi - \Upsilon_{\rm eff}/\Lambda$ plane by this constraint, with $m_\Psi < m_Z/2$. Then we confronted this area with the $\Upsilon_{\rm eff}/\Lambda$ values correctly reproducing the DM relic abundance Eq. (3) for each value of the dark fermion mass. For this operator, $B_{\mu\nu}\bar\Psi\sigma^{\mu\nu}\Psi$, we found both observables compatible in the whole region $m_\Psi < m_Z/2$.

We proceeded analogously with the $B^{\mu\nu}\bar\Psi(\gamma_\mu \overleftrightarrow{\mathcal{D}}_\nu - \gamma_\nu \overleftrightarrow{\mathcal{D}}_\mu)P_{L,R}\Psi$ operator, comparing the region allowed by the Z invisible decay width with the values of the effective coefficient $\kappa_{\rm eff}/\Lambda^2$ that correctly reproduce the observed relic abundance. We took $\kappa^L_{\rm eff} = \kappa^R_{\rm eff}$ to decrease the number of parameters. As we show in Fig. 1, we observe suitable solutions for $m_\Psi \gtrsim 20$ GeV.

We also contrasted these two observables using the operator $B_{\mu\nu}X^{\mu\nu}\Phi$. In this instance we find viable solutions for the full range $m_{\rm DM} < m_Z/2$, as long as $m_X = m_\Phi$ (when they differ by a few GeV or more, no solutions are found).

4. Observational limits

We will be discussing bounds obtained from several direct and indirect detection constraints; using the notation:

$$\begin{aligned}
&\text{OP1} \equiv B_{\mu\nu}\bar\Psi\sigma^{\mu\nu}\Psi,\\
&\text{OP2} \equiv \bar\psi\gamma^\mu\psi\bar\Psi\gamma_\mu P_{L,R}\Psi,\\
&\text{OP3} \equiv B_{\mu\nu}\bar\Psi(\gamma^\mu\mathcal{D}^\nu - \gamma^\nu\mathcal{D}^\mu)P_{L,R}\Psi,\\
&\text{OP4} \equiv B_{\mu\nu}X^{\mu\nu}\Phi,\\
&\text{OP5} \equiv \frac{1}{2i}\left(\bar\psi\gamma^\mu\psi\right)\left(\Phi^\dagger \overleftrightarrow{\partial}_\mu \Phi\right).
\end{aligned} \tag{5}$$

Couplings that properly reproduce the observed relic abundance, Eq. (3), will be used. For simplicity, we use first the single operator hypothesis, but we also consider the combined contributions from different operators when they share dark particle candidate (fermion, or scalar and vector); in those cases we use the following relationship between the operator coefficients C and the Λ scales:

$$C_{\rm dim6} = \pm C_{\rm dim5}\,, \qquad \Lambda_{\rm dim\,6} = \Lambda_{\rm dim\,5}. \tag{6}$$

We are using $\Lambda = 2\,m_{\rm DM}$ when combining operators of different dimensions[i], which is a conservative limit for the convergence of the effective theory [20].

4.1. Direct detection experiments

LUX-ZEPLIN [29], CRESST-III [30] and DarkSide-50 [31] experiments have derived the currently most stringent bounds on spin-independent scattering cross sections of nucleon-DM particles. However, we also include limits from the XENON1T [32] and PandaX-4T [33] experiments. Using micrOMEGAs [25], we study the implications for our effective theory with the DM-nucleon cross sections.

Figure 2 displays the values for the WIMP scattering cross sections per nucleon already ruled out by the direct detection experiments. This figure's notation is defined in Eq. (5). Unshown operators in Fig. 2 have values for the WIMP scattering cross sections per nucleon many orders of magnitude below current bounds from the discussed experiments. Thus, these will be the only ones considered in the following.

4.2. Limits from AMS-02 positron measurements

Positron fluxes and the positron fraction were measured by the AMS-02 collaboration. Reference [34] used the former to extract stringent limits on DM properties, and to derive limits on the lifetime for various final states and dark matter annihilation cross section. We computed the DM annihilation cross sections into e^+e^- and $\mu^+\mu^-$ using micrOMEGAs [25] and compared them with Ref. [34] bounds.

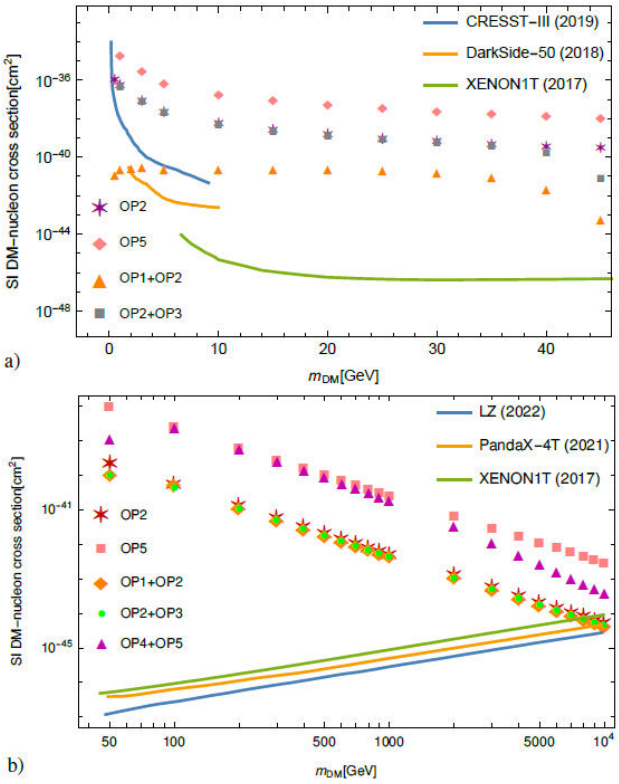

FIGURE 2. WIMP cross sections per nucleon for spin-independent coupling versus dark particle mass, a) $m_{\rm DM} < m_Z/2$, b) $m_{\rm DM} \in [50, 10000]$ GeV. Notation is defined in Eq. (5). Unshown operators —OP1, OP3, and the combination of OP1&OP3— have cross sections way below current limits.

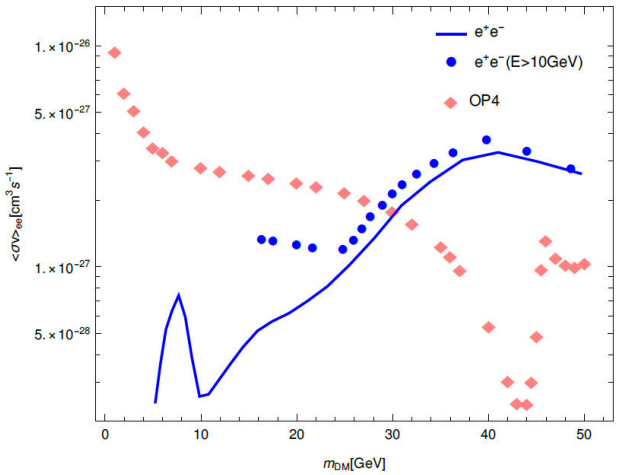

FIGURE 3. Restrictions from AMS-02 data on the DM annihilation cross sections into e^+e^-, for the portal generated by OP4, defined in Eq. (5). The dashed blue line was derived from considering intervals including only data with energies larger than 10 GeV, while the limits shown as a solid line were derived from sampling over various energy ranges [34]. This plot tests the mass region $m_\psi < m_Z/2$; masses smaller than ~ 30 GeV are not allowed.

The most stringent limits come from annihilation into e^+e^-; in Fig. 3 we compare them with the DM annihilation cross sections that we obtained using OP4. In this figure masses $\lesssim 30$ GeV are excluded by the data. Similar results are obtained using OP1, OP3 and the combination of OP1 & OP3, where masses $\lesssim 35$ GeV are excluded. Collider constraints will, however, set the most stringent bounds on our operators —along with direct detection limits that discard OP2, OP5 and several combinations of operators (see Fig. 2).

5. Collider constraints

WIMPs (χ) pair production in proton-proton collisions at the LHC is generated within our effective setting.

The process $pp \to \chi\chi j$ is produced when a jet is radiated through initial state radiation (ISR). It would be detected as a single jet together with missing transverse energy ($\not{E}_T$). Here, we include the ATLAS [35] monojet analysis based on 139 fb^{-1} of data from Run II.

We started using LanHEP v4.0.0 [36] to produce UFO files, then we use MadGraph_aMC@NLO v3.4.0 [37] to generate the process $pp \to \chi\chi j$, connected with Pythia v8.3 [38] for hadronization and parton showering. We used the ATLAS detector configuration [39] in FastJet v3.3.3 [40] to simulate the detector response. The kinematic cuts from Ref. [35] were applied.

ATLAS measurements were derived using proton-proton collision data at a center-of-mass energy of $\sqrt{s} = 13$ TeV.

Events were required to lack reconstructed photons or leptons and have at least one jet with transverse momentum above 200 GeV. The maximum mass that we considered in our simulations was 6.4 TeV, due to LHC center-of-mass energy.

We use the data points in Fig. 4 of ref. [35] of the measured distributions of $p_T^{\rm recoil}$. For example, in Fig. 4 we evaluated $m_\psi = 175$ GeV, 190 TeV and 225 GeV, and only masses larger than 190 GeV were allowed. We proceeded similarly

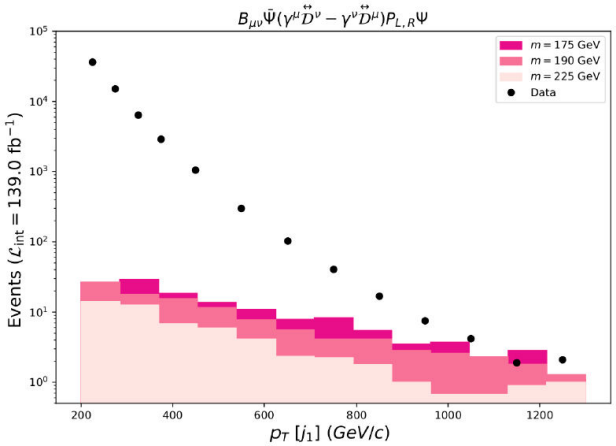

FIGURE 4. p_T distributions simulated using OP3 of Eq. (5), vs ATLAS data [35]. We use benchmark points for 175 GeV, 190 GeV and 225 GeV. Masses smaller than 190 GeV are ruled out.

TABLE I. Summary of our results. The $(m_Z \pm \Gamma_Z)/2$ region is excluded by indirect detection limits (see the main text for further details).

Operator	Dim.	DM candidate	Allowed DM mass (GeV)
1.- $B_{\mu\nu}\bar{\Psi}\sigma^{\mu\nu}\Psi$	5	fermion Ψ	$\gtrsim 43$ *
2.- $\left(\bar{\psi}\gamma_\mu\psi\right)\left(\bar{\Psi}\gamma^\mu P_{L,R}\Psi\right)$	6	fermion Ψ	none
3.- $B_{\mu\nu}\bar{\Psi}(\gamma^\mu \overleftrightarrow{\mathcal{D}}^\nu - \gamma^\nu \overleftrightarrow{\mathcal{D}}^\mu)P_{L,R}\Psi$	6	fermion Ψ	$\gtrsim 190$
4.- $B_{\mu\nu}X^{\mu\nu}\Phi$	5	vector X, scalar Φ	$m_X \sim m_\Phi \gtrsim 30$ *
5.- $\left(\bar{\psi}\gamma_\mu\psi\right)\frac{1}{2i}\Phi^\dagger \overleftrightarrow{\mathcal{D}}^\mu \Phi$	6	scalar Φ	none
1 ± 2	5+6	fermion Ψ	none
$1 + 3$	5+6	fermion Ψ	$\gtrsim 325$
$1 - 3$	5+6	fermion Ψ	$\gtrsim 140$
2 ± 3	6	fermion Ψ	none
4 ± 5	5+6	vector X, scalar Φ	none

using the operators that still had allowed mass regions — OP1, OP3, OP4 and the combination of OP1& OP3—. We show our results next.

6. Discussion and conclusions

Our results are summarized in Table I.

The combination of collider constraints together with direct detection experiments bind stringently our operators. The constraining capacity of ATLAS measurements excludes mainly DM particles with mass smaller than the electroweak scale. Apart from a window below m_Z for OP1 and OP4, remaining solutions (for OP1, OP3 and OP1$\pm$OP3) are viable only for DM masses around the electroweak scale and above. Future LHC analyses will clearly increase our reach on WIMP DM, particularly within the setting studied here.

Acknowledgements

F. F. is grateful to Conahcyt for funding. It is my pleasure to thank Pablo Roig and José Wudka for a fruitful collaboration and insightful discussions and Marco A. Arroyo-Ureña for his useful help with the software employed in these studies.

i. Except for the masses $m_{\rm DM} < m_Z/2$, where we employed two values of Λ as benchmark points, $\Lambda = 230$ GeV and $\Lambda = 1$ TeV. However, since the value of Λ mainly impacts the subdominant operator, its effects are negligible.

1. F. Fortuna, P. Roig, and J. Wudka, Effective field theory analysis of dark matter-standard model interactions with spin one mediators, *JHEP* **2021** (2021) 223, https://doi.org/10.1007/JHEP02(2021)223.

2. F. Fortuna and P. Roig, Impact of ATLAS constraints on effective dark matter-standard model interactions with spin-one mediators, *Phys. Rev. D* **107** (2023) 075003, https://doi.org/10.1103/PhysRevD.107.075003.

3. G. Arcadi *et al.*, The waning of the WIMP? A review of models, searches, and constraints, *Eur. Phys. J. C* **78** (2018) 203, https://doi.org/10.1140/epjc/s10052-018-5662-y.

4. L. Roszkowski, E. M. Sessolo, and S. Trojanowski, WIMP dark matter candidates and searches-current status and future prospects, *Rept. Prog. Phys.* **81** (2018) 066201, https://doi.org/10.1088/1361-6633/aab913.

5. G. Bélanger *et al.*, Dark matter direct detection rate in a generic model with micrOMEGAs 2.2, *Comput. Phys. Commun.* **180** (2009) 747, https://doi.org/10.1016/j.cpc.2008.11.019.

6. A. Crivellin and U. Haisch, Dark matter direct detection constraints from gauge bosons loops, *Phys. Rev. D* **90** (2014) 115011, https://doi.org/10.1103/PhysRevD.90.115011.

7. B. Barman *et al.*, Effective Leptophilic WIMPs at the e^+e^- collider, *JHEP* **2022** (2022) 146, https://doi.org/10.1007/JHEP04(2022)146.

8. A. Crivellin, F. D'Eramo, and M. Procura, New Constraints on Dark Matter Effective Theories from Standard Model Loops, *Phys. Rev. Lett.* **112** (2014) 191304, https://doi.org/10.1103/PhysRevLett.112.191304.

9. M. Duch, B. Grzadkowski, and J. Wudka, Classification of effective operators for interactions between the Standard Model and dark matter, *JHEP* **2015** (2015) 116, https://doi.org/10.1007/JHEP05(2015)116.

10. J. Goodman *et al.*, Constraints on Dark Matter from Colliders, *Phys. Rev. D* **82** (2010) 116010, https://doi.org/10.1103/PhysRevD.82.116010.

11. S. Bhattacharya and J. Wudka, Effective theories with dark matter applications, *Int. J. Mod. Phys. D* **30** (2021) 2130004, https://doi.org/10.1142/S0218271821300044.

12. V. Gonzéalez Macías and J. Wudka, Effective theories for Dark Matter interactions and the neutrino portal paradigm, *JHEP* **2015** (2015) 161, https://doi.org/10.1007/JHEP07(2015)161.
13. G. Bertone, D. Hooper, and J. Silk, Particle dark matter: Evidence, candidates and constraints, *Phys. Rept.* **405** (2005) 279, https://doi.org/10.1016/j.physrep.2004.08.031.
14. J. L. Feng, Dark Matter Candidates from Particle Physics and Methods of Detection, *Ann. Rev. Astron. Astrophys.* **48** (2010) 495, https://doi.org/10.1146/annurev-astro-082708-101659.
15. D. Racco, A. Wulzer, and F. Zwirner, Robust collider limits on heavy-mediator Dark Matter, *JHEP* **05** (2015) 009, https://doi.org/10.1007/JHEP05(2015)009.
16. N. F. Bell, *et al*., Dark matter at the LHC: Effective field theories and gauge invariance, Phys. *Rev. D* **92** (2015) 053008, https://doi.org/10.1103/PhysRevD.92.053008.
17. A. De Simone and T. Jacques, Simplified models vs. effective field theory approaches in dark matter searches, *Eur. Phys. J. C* **76** (2016) 367, https://doi.org/10.1140/epjc/s10052-016-4208-4.
18. Q.-H. Cao, et al., Effective Dark Matter Model: Relic density, CDMS II, Fermi LAT and LHC, *JHEP* **08** (2011) 018, https://doi.org/10.1007/JHEP08(2011)018.
19. K. Cheung, *et al*., Global Constraints on Effective Dark Matter Interactions: Relic Density, Direct Detection, Indirect Detection, and Collider, *JCAP* **1205** (2012) 001, https://doi.org/10.1088/1475-7516/2012/05/001.
20. G. Busoni *et al*., On the Validity of the Effective Field Theory for Dark Matter Searches at the LHC, *Phys. Lett. B* **728** (2014) 412, https://doi.org/10.1016/j.physletb.2013.11.069.
21. O. Buchmueller *et al.*, Characterising dark matter searches at colliders and direct detection experiments: Vector mediators, *JHEP* **01** (2015) 037, https://doi.org/10.1007/JHEP01(2015)037.
22. B. Patt and F. Wilczek, Higgs-field portal into hidden sectors (2006), https://arxiv.org/abs/hep-ph/0605188.
23. V. González-Macías, J. I. Illana, and J. Wudka, A realistic model for Dark Matter interactions in the neutrino portal paradigm, *JHEP* **2016** (2016) 171, https://doi.org/10.1007/JHEP05(2016)171.
24. J. M. Lamprea *et al.*, Self-interacting neutrino portal dark matter, *Phys. Rev. D* **103** (2021) 015017, https://doi.org/10.1103/PhysRevD.103.015017.
25. G. Bélanger *et al.*, micrOMEGAs4.1: two dark matter candidates, *Comput. Phys. Commun.* **192** (2015) 322, https://doi.org/10.1016/j.cpc.2015.03.003.
26. P. Zyla *et al.*, Review of Particle Physics, *PTEP* **2020** (2020) 083C01, https://doi.org/10.1093/ptep/ptaa104.
27. P. Janot and S. Jadach, Improved Bhabha cross section at LEP and the number of light neutrino species, *Phys. Lett. B* **803** (2020) 135319, https://doi.org/10.1016/j.physletb.2020.135319.
28. M. Tanabashi *et al.*, Review of Particle Physics, *Phys. Rev. D* **98** (2018) 030001, https://doi.org/10.1103/PhysRevD.98.030001.
29. J. Aalbers *et al*., First Dark Matter Search Results from the LUX-ZEPLIN (LZ) Experiment (2022), https://arxiv.org/abs/2207.03764.
30. A. H. Abdelhameed *et al*., First results from the CRESSTIII low-mass dark matter program, *Phys. Rev. D* **100** (2019) 102002, https://doi.org/10.1103/PhysRevD.100.102002.
31. P. Agnes *et al*., Low-Mass Dark Matter Search with the DarkSide-50 Experiment, *Phys. Rev. Lett.* **121** (2018) 081307, https://doi.org/10.1103/PhysRevLett.121.081307.
32. E. Aprile *et al*., Dark Matter Search Results from a One Ton-Year Exposure of XENON1T, *Phys. Rev. Lett.* **121** (2018) 111302, https://doi.org/10.1103/PhysRevLett.121.111302.
33. Y. Meng *et al.*, Dark Matter Search Results from the PandaX- 4T Commissioning Run, *Phys. Rev. Lett*. **127** (2021) 261802, https://doi.org/10.1103/PhysRevLett.127.261802.
34. A. Ibarra, A. S. Lamperstorfer, and J. Silk, Dark matter annihilations and decays after the AMS-02 positron measurements, *Phys. Rev. D* **89** (2014) 063539, https://doi.org/10.1103/PhysRevD.89.063539.
35. G. Aad *et al*., Search for new phenomena in events with an energetic jet and missing transverse momentum in pp collisions at $\sqrt{s} = 13$ TeV with the ATLAS detector, *Phys. Rev. D* **103** (2021) 112006, https://doi.org/10.1103/PhysRevD.103.112006.
36. A. Semenov, LanHEP - A package for automatic generation of Feynman rules from the Lagrangian. Version 3.2, *Comput. Phys. Commun.* **201** (2016) 167, https://doi.org/10.1016/j.cpc.2016.01.003.
37. J. Alwall *et al*., The automated computation of tree-level and next-to-leading order differential cross sections, and their matching to parton shower simulations, *JHEP* **2014** (2014) 079, https://doi.org/10.1007/JHEP07(2014)079.
38. C. Bierlich *et al*., A comprehensive guide to the physics and usage of PYTHIA **8.3** (2022), https://doi.org/10.21468/SciPostPhysCodeb.8.
39. J. Y. Araz, B. Fuks, and G. Polykratis, Simplified fast detector simulation in MADANALYSIS 5, *Eur. Phys. J. C* **81** (2021) 329, https://doi.org/10.1140/epjc/s10052-021-09052-5.
40. M. Cacciari, G. P. Salam, and G. Soyez, FastJet User Manual, *Eur. Phys. J. C* **72** (2012) 1896, https://doi.org/10.1140/epjc/s10052-012-1896-2.